

基于瑞利图形相关的光纤分布式动态应变传感器

王一凡, 刘庆文^{*}, 李赫, 陈典, 何祖源^{**}

上海交通大学区域光纤通信网与新型光通信系统国家重点实验室, 上海 200240

摘要 基于背向瑞利散射和啁啾探测脉冲的分布式光纤传感器, 能够利用单个探测脉冲获取待测光纤的瑞利散射频谱, 突破测量精度与空间分辨率之间的矛盾, 实现动态应变信号的测量。瑞利散射频移的检测是应变传感的关键, 为此, 提出了一种基于频率轴方向的瑞利频移检测方案, 与之前距离轴方向的瑞利频移检测方案相比, 该方案利用了更多的瑞利频谱特征信息, 进一步提高了应变信号测量的信噪比。在验证实验中, 该方案成功还原出在 10 km 待测光纤末端上施加的幅度为 100 nm 的正弦振动波形, 系统的空间分辨率为 1 m, 应变分辨率为 157 pm/√Hz, 在不需任何平均处理下, 信噪比达到 32.5 dB。

关键词 光纤光学; 分布式光纤传感; 瑞利散射

中图分类号 TN247

文献标志码 A

doi: 10.3788/CJL202148.1110002

1 引言

基于后向瑞利散射的分布式光纤动态应变传感器可以对光纤上的动态应变事件进行定位检测和定量解调^[1-3]。由于其具有本征安全、感知与传输一体、工作距离长、灵敏度高、鲁棒性好等特点, 在管道泄漏监控、桥梁安全检测等领域有着其他方法无法取代的优势^[4-6]。根据解调方式不同, 基于后向瑞利散射的传感器可以分为相位解调和频率解调两类。相位解调型光纤传感器利用的是应变变化和瑞利散射光相位变化之间的线性关系^[7-9], 计算量较小、空间分辨率高, 广泛用于分布式声波信号传感领域; 但由于瑞利散射的相位是以 2π 为周期的函数, 在应变较大时, 无法根据相位唯一确定应变值, 因此只适用于小振幅信号的检测^[10-12], 而难以实现准静态及大应变的测量。

基于瑞利散射频谱的分布式光纤传感器利用的是应变会引起光纤瑞利散射频谱的改变, 且频谱的改变量正比于应变大小的特性。这种方式既能测量静态应变也能测量动态应变, 而且解调方式决定了它不存在相位型传感器的干涉衰落噪声问题^[13-15], 因而得到了广泛的发展和应用。2009 年, Koyamada 等^[16]提出了步进式扫频进行强度解调的

方式来得到不同光频率对应的瑞利背向散射光的强度图形的方法, 但是由于这种方式的测量周期过长, 导致系统的响应带宽成倍地降低, 因此只能测量温度或者频率很低的应变事件。2016 年 Graells 等^[17]提出利用啁啾脉冲代替步进式扫频的方案, 有效改善了系统的响应带宽问题, 但是由于传感距离和空间分辨率之间的固有矛盾, 系统的空间分辨率还有待提高。本课题组在之前的工作中^[18], 提出了使用啁啾脉冲和匹配滤波的方式, 获得待测光纤在不同中心频率下瑞利散射的强度曲线, 并将该曲线与事先建立的瑞利曲线数据库比较求得应变信号。系统的空间分辨率由于匹配滤波器的引入得到了较大的提升, 但这种方法需要事前建立待测光纤的数据库, 并且计算过程中每个位置处都需要大量的互相关运算以实现瑞利图形的匹配, 限制了系统性能的进一步提升。

本文在课题组前述工作的基础上, 改进了数据处理方法, 提出了一种在频率轴上检测瑞利图形位移来求解应变的方法, 不仅保留了原测量方案中空间分辨率高、测量速度快的优点, 而且避免了提前建立数据库的要求, 减小了计算量, 并进一步提升了系统的应变测量信噪比(SNR)。

收稿日期: 2020-10-18; 修回日期: 2021-11-15; 录用日期: 2020-12-14

基金项目: 国家重点研发计划(2018YFC1503703)、国家自然科学基金(61875121, 61620106015)

*E-mail: liuqingwen@sjtu.edu.cn; **E-mail: zuyuanhe@sjtu.edu.cn

2 实验原理和装置

实验系统装置示意图如图 1 所示,窄带宽激光器光源发射的光波经过 1 : 99 保偏耦合器后分成本地光和探测光两路,其中,光强较强的一路为探测光,经过强度调制器(IM)后产生载波和正负边带信号。该强度调制器由任意波形发生器(AWG)驱动,任意波形发生器产生的啁啾脉冲信号表达式为

$$S_0(t) = \text{rect}\left(\frac{t}{t_c}\right) \exp\{j[2\pi f_0 t + \pi K t^2]\}, \quad (1)$$

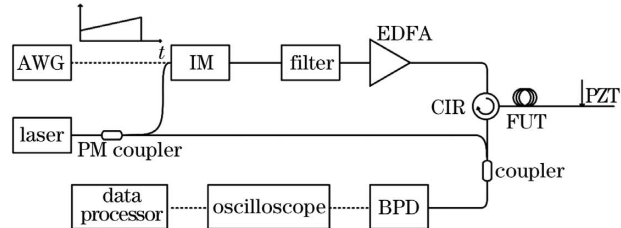


图 1 实验系统装置图

Fig. 1 Experimental system setup diagram

式中: t_c 为脉冲宽度; $\text{rect}(t/t_c)$ 为 $t \in [0, t_c]$ 的矩形窗函数; f_0 为啁啾脉冲的初始频率; K 为啁啾速率。本次实验采用的啁啾信号频率范围为 [200 MHz, 750 MHz], 脉冲持续时间为 4 μs 。探测光经滤波器滤除载波和负边带后,留下正边带信号再经掺铒光纤放大器(EDFA)放大后进入待测光纤(FUT)。返回的瑞利背向散射光经光环形器后与本地光混合,被平衡探测器(BPD)接收并输出拍频信号。拍频信号的表达式为

$$i(t) = \int_0^{T_p} a(\tau) r(\tau) \text{rect}\left(\frac{t-\tau}{t_c}\right) \exp\{j[2\pi f_0(t-\tau) + \pi K(t-\tau)^2 - 2\pi f_c \tau]\} d\tau, \quad (2)$$

式中: T_p 为光波在待测光纤中的最大往返时间; τ 为瑞利背向散射光从输入位置到散射点位置的往返时间; $a(\tau)$ 为光纤衰减系数; $r(\tau)$ 为后向瑞利散射系数。

平衡光电探测器输出的拍频信号经过数据采集卡转为数字信号。在数据处理中,系统生成相应的匹配滤波器对拍频数据进行匹配滤波。采用的匹配滤波器的中心频率决定了滤出信号的中心频率,滤波器的带宽决定了滤出信号的空间分辨率,滤波器中心频率的间隔决定了滤出信号的频率分辨率^[12]。这打破了光纤中空间分辨率和传感距离之间的矛盾,可以同时实现较高的空间分辨率和信噪比。

本次实验所发射的探测光信号相对于激光器原始波长的频率调制范围为 [200 MHz, 750 MHz]。在接收端,生成了 91 个频带宽度均为 100 MHz、彼

此之间的频率步进间隔为 5 MHz 的匹配滤波器对接收到的拍频数据进行匹配滤波,滤波的结果是得到了待测光纤在(相对于激光器原始波长)中心频率分别为 250, 255, 260, …, 700 MHz 的单频探测光对应的瑞利强度信号,其空间分辨率为 1 m。因此,对待测光纤上每个位置 z (覆盖一个空间分辨率的范围),利用一个探测脉冲即可以获得该位置在 91 个间隔为 5 MHz 的探测光所产生的瑞利强度值。该方案与分 91 次发射单频信号的步进式扫频相比具有同样的结果,因而显著缩短了测量的周期,提升了系统的响应带宽。为了进一步增加频率分辨率,对这些单频瑞利信号在频率方向上进行了 50 倍三次样条插值,从而得到频率间隔为 0.1 MHz 的瑞利强度曲线。对接收到的每一个脉冲的数据进行同样的滤波和插值操作。本实验发射的啁啾脉冲数量为 200 个,每个脉冲时间持续时间 $t_c = 4 \mu\text{s}$,脉冲发射周期为 100 μs ,由奈奎斯特定理可得到本系统的响应带宽为 5 kHz。

3 基于瑞利图形的应变解调

光纤在外界应变作用下引起的瑞利强度谱的变化,与探测光频率改变所引起强度谱变化等效。提取各个啁啾脉冲在光纤上同一位置 z 处频率强度曲线,如果光纤在此期间受到了外加应变,则各啁啾脉冲产生的瑞利图形在频率轴上会产生平移。通过在频率轴上对各啁啾探测脉冲的瑞利强度谱频率曲线进行互相关运算,求出对应强度曲线在频率轴上的移动量,即可以计算得到光纤所受应变的大小。

在实验系统中,待测光纤的长度为 10 km,从 9967 m 处开始,我们利用压电陶瓷平台,在长度为 10 m 的光纤上,施加了频率为 800 Hz 的正弦应变信号。图 2 展示了不同探测脉冲在 9970 m 处、[250 MHz, 700 MHz] 频率范围内的瑞利散射强度曲线,图中不同的颜色和线型代表了不同的脉冲曲线。从图 2 可以看到,在光纤上施加应变的作用下,各探测脉冲所得到的瑞利图形相对于第一个探测脉冲(视为初始状态)的频率差也在逐渐发生变化。利用互相关系数表达式,可以求出两个脉冲的频率强度曲线之间的频率变化。

$$P_{i,j}(f_s) = \frac{\sum_{z,f} [I_i(f_s) - \overline{I_i(f_s)}][I_j(f_s) - \overline{I_j(f_s)}]}{\sqrt{\sum_f [I_i(f_s) - \overline{I_i(f_s)}]^2 \sum_f [I_j(f_s) - \overline{I_j(f_s)}]^2}}, \quad (3)$$

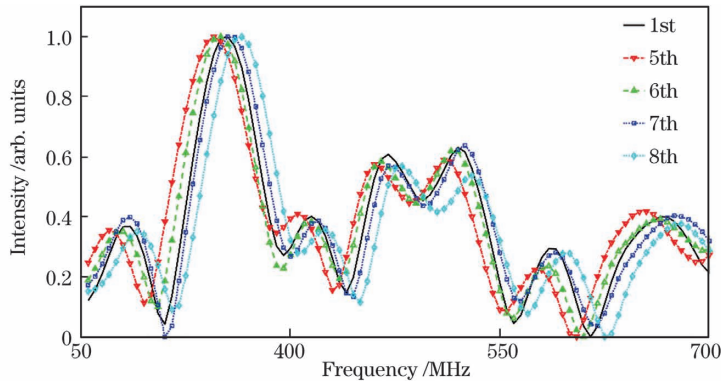


图 2 同一位置处第 5~8 个探测脉冲与第 1 个探测脉冲瑞利频谱的对比

Fig. 2 Comparison of the Rayleigh spectra of the 5th to 8th probe pulses and the first probe pulse at the same position

式中: $I_i(f_s)$ 代表第 i 个脉冲在位置 z 的频率强度曲线; $\overline{I_i(f_s)}$ 为强度矩阵的平均值; $P_{i,j}(f_s)$ 代表在位置 z 处第 i 个脉冲和第 j 个脉冲之间的互相关系数。在进行互相关运算的时候,一条强度曲线保持不动,另一条进行步进式移动,然后求出每一个移动位置的互相关系数,当互相关系数达到最大时,其对应的频率偏移就是第 i 个脉冲和第 j 个脉冲之间频率的偏移量。

在使用互相关运算求出这两个脉冲之间频率的变化之后,再利用频率变化与应变之间的关系可以

求出其对应的应变波形,关系表达式为^[16]

$$\frac{\Delta v}{v_0} = \frac{\Delta n}{n_0} = -K_\epsilon \Delta \epsilon \approx -0.78 \Delta \epsilon, \quad (4)$$

式中: K_ϵ 代表应变系数; v_0 代表归一化频率; n_0 代表有效折射率。因为应变测量精度和频率分辨率有关,所以需要在预处理时在频率轴方向上使用三次样条插值来提升应变测量分辨率。图 3 展示了使用 50 倍三次样条插值和未使用插值在光纤 9970 m 处解调出的应变波形的对比,可以看到,未使用插值时由于频率分辨率比较低,导致波形不够光滑,信噪比也较低。

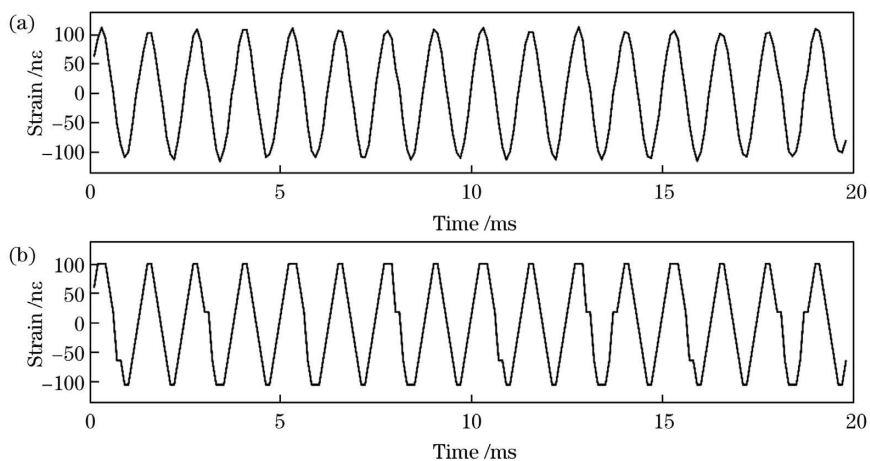


图 3 应变波形对比。(a) 使用三次样条插值;(b) 未使用三次样条插值

Fig. 3 Comparison of strain waveforms. (a) With cubic spline interpolation; (b) without cubic spline interpolation

图 4 展示了最终的实验结果,图 4(a)由每个脉冲和第一个脉冲的互相关曲线组成,可以看到正弦应变的信号,通过此应变信号的功率谱密度可以求得其信噪比为 32.5 dB,如图 4(b)所示。图 4(c)为沿着光纤上频率偏移的情况,图 4(d)为其标准差(SD)曲线,从图中可以观察到,从最高高度的 10% 到 90% 对应的光纤长度约为 1 m,这与前面提到的理论空间分辨率 1 m 相一致。系统的应变分辨率

为 $157 \text{ p}\epsilon/\sqrt{\text{Hz}}$ 。

如表 1 所示,与文献[18]中的基于光纤距离方向的瑞利特征匹配法相比,本实验方案中基于频率轴的瑞利图形相关法有以下优势:瑞利特征匹配法是以第一个脉冲的所有频率的特征曲线建立了数据库,之后每一个脉冲都需要通过大量的互相关运算来求出和数据库中最相似的特征;但是在基于频率轴的方法中,同一位置在不同探测脉冲下的瑞利强

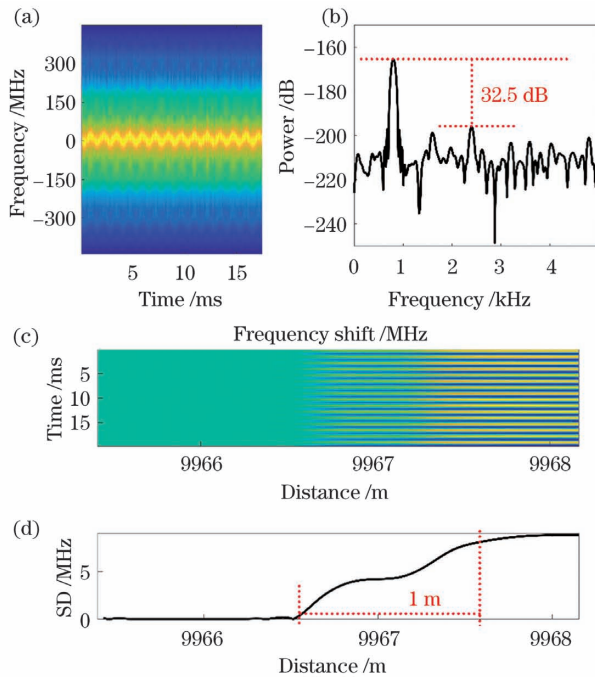


图4 应变信号解调结果。(a)在20 ms内的应变信号;(b)应变的功率谱密度,可得到信噪比约为32.5 dB;(c)待测光纤末端随着时间变化的频率偏移,图中的条纹代表该位置处发生了振动;(d)对(c)求光纤上每个位置的标准差,上升沿的10%~90%对应的横坐标上的距离也就是实际的空间分辨率,约为1 m

Fig. 4 Results of strain demodulation. (a) Strain signal in 20 ms; (b) power spectral density of strain signal, where the SNR is 32.5 dB; (c) frequency shift at near end of fiber, the stripes represent vibration at this position; (d) standard deviation of (c) on each point of fiber, where the distance between 10% and 90% of the edge is about 1 m, which is also the spatial resolution of the system

表1 沿光纤距离轴方向和沿频率轴方向的解调方法的性能对比

Table 1 Performance comparison of demodulation methods along fiber axial direction and frequency axis direction

Direction	Spatial resolution / m	SNR / dB	Strain resolution / $(\mu\epsilon/\sqrt{Hz})$	Measurement time / s
Distance axis	0.9	25.7	237	4.5
Frequency axis	1.0	32.5	157	0.8

度图形具有相同的形状,应变信号对应于两条曲线的位置移动,因此只需要在相邻脉冲之间进行一次互相关运算即可得到应变值,大大减小了互相关运算的次数;同时由于利用了每个脉冲在不同频率上的强度信息,更多的瑞利信息也提升了应变信号的信噪比;当光纤受到应变时,瑞利曲线移动的同时,频率范围也得到扩展,因此可以逐步扩展数据库,从而实现对缓慢变化的大信号的测量。

4 结 论

本文提出了一种根据瑞利强度谱的频率偏移解调应变的分布式应变传感技术。这种技术在之前基于啁啾脉冲和匹配滤波器的方案上进一步提高了系统的信噪比。所提出的频率轴上检测强度频谱移动

的数据处理算法,不仅降低了计算量,而且能够充分利用瑞利图形信息,进一步提升了系统的信噪比。结合其高空间分辨率、高响应带宽、高信噪比、应变量程大等优点,该方案具有广泛的应用前景。

参 考 文 献

- [1] Juarez J C, Maier E W, Choi K N, et al. Distributed fiber-optic intrusion sensor system [J]. Journal of Lightwave Technology, 2005, 23(6): 2081-2087.
- [2] Cai H W, Ye Q, Wang Z Y, et al. Distributed optical fiber acoustic sensing technology based on coherent Rayleigh scattering [J]. Laser & Optoelectronics Progress, 2020, 57(5): 050001.
蔡海文,叶青,王照勇,等.基于相干瑞利散射的分布式光纤声波传感技术[J].激光与光电子学进展,2020,57(5):050001.

- [3] He Z Y, Liu Q W, Chen D, et al. Advances in fiber-optic distributed acoustic sensors [C] // 2018 23rd Opto-Electronics and Communications Conference (OECC), July 2-6, 2018, Jeju, Korea (South). New York: IEEE Press, 2018: 1-2.
- [4] Wang C, Liu Q W, Chen D, et al. Monitoring pipeline leakage using fiber-optic distributed acoustic sensor [J]. *Acta Optica Sinica*, 2019, 39 (10): 1006005.
王辰, 刘庆文, 陈典, 等. 基于分布式光纤声波传感的管道泄漏监测 [J]. 光学学报, 2019, 39 (10): 1006005.
- [5] Wu T, Yang C Y, Shang J C, et al. Influences of correlation parameter errors on accurate measurement of gas temperature based on spontaneous Rayleigh-Brillouin scattering [J]. *Acta Optica Sinica*, 2019, 39 (9): 0912006.
吴涛, 杨传音, 商景诚, 等. 基于自发瑞利-布里渊散射的相关参数误差对气体温度准确测量的影响 [J]. 光学学报, 2019, 39(9): 0912006.
- [6] Ma H Y, Wang X X, Ma F, et al. Research progress of Φ -OTDR distributed optical fiber acoustic sensor [J]. *Laser & Optoelectronics Progress*, 2020, 57 (13): 130005.
马皓钰, 王夏霄, 马福, 等. Φ -OTDR型分布式光纤声波传感器研究进展 [J]. 激光与光电子学进展, 2020, 57(13): 130005.
- [7] Dong Y K, Chen X, Liu E H, et al. Quantitative measurement of dynamic nanostrain based on a phase-sensitive optical time domain reflectometer [J]. *Applied Optics*, 2016, 55(28): 7810-7815.
- [8] Chen D, Liu Q W, He Z Y, et al. Distributed fiber-optic acoustic sensor with long sensing range over 100 km and sub-nano strain resolution [C] // 2019 IEEE International Instrumentation and Measurement Technology Conference (I2MTC), May 20-23, 2019, Auckland, New Zealand. New York: IEEE Press, 2019: 1-5.
- [9] Chen D, Liu Q W, Wang Y F, et al. Fiber-optic distributed acoustic sensor based on a chirped pulse and a non-matched filter [J]. *Optics Express*, 2019, 27(20): 29415-29424.
- [10] Pan Z Q, Liang K Z, Ye Q, et al. Phase-sensitive OTDR system based on digital coherent detection [J]. *Proceedings of SPIE*, 2011, 8311: 83110S.
- [11] Chen D, Liu Q W, He Z Y, et al. Fading-suppressed distributed fiber-optic acoustic sensor with 0.8-m spatial resolution and $246\text{-pe}/\sqrt{\text{Hz}}$ strain resolution [C] // Optical Fiber Sensors 2018, September 24-28, 2018, Lausanne Switzerland. Washington D.C.: OSA, 2018: TuE93.
- [12] Chen D, Liu Q W, Fan X Y, et al. Fading-noise-free distributed fiber-optic vibration sensor based on time-gated digital OFDR [C] // Asia Pacific Optical Sensors Conference, October 11-14, 2016, Shanghai, China. Washington, D.C.: OSA, 2016: W4A.2.
- [13] Pan Z Q, Liang K Z, Zhou J, et al. Interference-fading-free phase-demodulated OTDR system [J]. *Proceedings of SPIE*, 2012, 8421: 842129.
- [14] Chen D, Liu Q W, He Z Y, et al. Phase-detection distributed fiber-optic vibration sensor without fading-noise based on time-gated digital OFDR [J]. *Optics Express*, 2017, 25(7): 8315-8325.
- [15] Chen D, Liu Q W, Fan X Y, et al. Distributed fiber-optic acoustic sensor with enhanced response bandwidth and high signal-to-noise ratio [J]. *Journal of Lightwave Technology*, 2017, 35 (10): 2037-2043.
- [16] Koyamada Y, Imahama M, Kubota K, et al. Fiber-optic distributed strain and temperature sensing with very high measurand resolution over long range using coherent OTDR [J]. *Journal of Lightwave Technology*, 2009, 27(9): 1142-1146.
- [17] Graells J P, Martins H F, Ruiz A G, et al. Single-shot distributed temperature and strain tracking using direct detection phase-sensitive OTDR with chirped pulses [J]. *Optics Express*, 2016, 24 (12): 13121-13133.
- [18] Wang Y F, Liu Q W, Chen D, et al. Distributed fiber-optic dynamic-strain sensor with sub-meter spatial resolution and single-shot measurement [J]. *IEEE Photonics Journal*, 2019, 11(6): 1-8.

Distributed Fiber-Optic Dynamic Strain Sensor Based on Spectra Correlation of Rayleigh Backscattering

Wang Yifan, Liu Qingwen*, Li He, Chen Dian, He Zuyuan**

State Key Laboratory of Advanced Optical Communication Systems and Networks,
Shanghai Jiao Tong University, Shanghai 200240, China

Abstract

Objective The distributed fiber-optic strain sensor based on the spectra of Rayleigh backscattering can detect static and dynamic signals. In addition, it is immune to interference fading. The Rayleigh scattering spectra of the optical fiber can be obtained using single-shot detection with frequency chirped pulses and matched filters; this solves the contradiction between spatial resolution and sensing distance. The frequency shift detection of Rayleigh scattering is the key in strain sensing. In this study, a Rayleigh frequency shift detection algorithm based on the frequency axis is proposed and verified in a configuration with chirped pulses and matched filters. Compared with the Rayleigh frequency shift detection algorithm on the distance axis, the signal-to-noise ratio is improved by more than 6 dB in dynamic strain measurement.

Methods The proposed system is based on a time-gated digital optical frequency domain reflectometer (TGD-OFDR) configuration (Fig. 1). Light wave from a narrow line-width fiber laser is split into local light and probe light. A filter is used to select the required sideband and suppress high-order harmonics. An erbium-doped fiber amplifier is used to boost the power of the probe pulse. The beat frequency between the Rayleigh backscattering and local oscillator from the balanced photo-detectors is sampled using an oscilloscope. Then, 91 matched filters with a frequency range and interval of 100 MHz and 5 MHz, respectively, are used to filter the beat signals, by which the Rayleigh scattering curves of different frequencies are obtained. At the position where the strain occurs, the spectral shift of Rayleigh backscattering on the frequency axis can be demodulated using a cross-correlation algorithm. The corresponding strain changes can be calculated using this frequency shift. Further, the strain waveform is obtained.

Results and Discussions The proposed distributed dynamic strain intensity-demodulation system successfully detects the strain on the optical fiber. By calculating the spectra of different pulses at the same position, the strain changes between pulses can be obtained (Fig. 2). To reduce the frequency interval, cubic spline interpolation is used before the cross-correlation algorithm for better strain resolution (Fig. 3). In the demonstrational experiment, 200 chirped pulses were launched into the fiber in sequence. The frequency-sweeping range of the probe pulse is from 200 MHz to 750 MHz. The width of each pulse is 4 μ s, and the measurement period is 100 μ s. The sinusoidal vibration with an amplitude of 100 nm applied to the far end of the 10 km fiber was successfully retrieved. The system's spatial resolution is evaluated by the distribution of the standard deviation of the frequency shift. The distance between 10% and 90% of the rising edge of the vibration area is approximately 1 m, which is the system's spatial resolution (Fig. 4). Compared with the intensity-demodulation method based on the distance axis, in this system, signal-to-noise ratio is improved from 25.7 dB to 32.5 dB and the frequency resolution is improved from 237 ps/ $\sqrt{\text{Hz}}$ to 157 ps/ $\sqrt{\text{Hz}}$. The main reason for performance improvement is the usage of more Rayleigh feature information. Moreover, data processing time is reduced from 4.5 s to 0.8 s (Table 1).

Conclusions In this study, a distributed strain-sensing technique based on frequency shift of Rayleigh spectrum is proposed. The use of chirped pulses and matched filters eliminates the contradiction between spatial resolution and dynamic range, where the system's spatial resolution is obtained using the frequency range instead of the pulse width. Compared with the spectral demodulation on the distance axis, the proposed data processing algorithm can reduce the amount of calculation and make full use of Rayleigh graphic information to improve the signal-to-noise ratio of the system. Combined with the advantages of high spatial resolution, high response bandwidth, high signal-to-noise ratio, and large strain range, the scheme has great potential in dynamic strain-sensing applications.

Key words fiber optics; distributed fiber sensor; Rayleigh scattering

OCIS codes 060.2370; 060.2840